CARBON 69 (2014) 444–451

Available at www.sciencedirect.com

ScienceDirect

journal homepage: www.elsevier.com/locate/carbon

Cycle and rate performance of chemically modified super-aligned carbon nanotube electrodes for lithium ion batteries

*Mengya Li, Yang Wu *, Fei Zhao, Yang Wei, Jiaping Wang *, Kaili Jiang, Shoushan Fan*

Department of Physics & Tsinghua-Foxconn Nanotechnology Research Center, Tsinghua University, Beijing 100084, People's Republic of China

ARTICLE INFO

Article history:
Received 6 October 2013
Accepted 15 December 2013
Available online 19 December 2013

ABSTRACT

Super-aligned multi-walled carbon nanotubes (MWCNTs), which had been produced in large-scale, were oxidized by H_2O_2 and HNO_3. The surface defects and oxygen-containing functional groups introduced during the oxidizing process were characterized by Raman spectroscopy and X-ray photoelectron spectroscopy. The surface modification of MWCNTs improved the electrochemical properties. As a result, H_2O_2-treated and HNO_3-treated MWCNTs displayed reversible capacities of 364 mA h/g and 391 mA h/g, respectively, after 80 galvanostatic cycles, corresponding to 143% and 154% improvements compared with pristine MWCNTs. The rate capability was also increased. At a current density of 3500 mA/g, H_2O_2-treated and HNO_3-treated MWCNTs exhibited reversible capacities of 66 mA h/g and 156 mA h/g, respectively. In contrast, pristine MWCNTs were only able to deliver 27 mA h/g at this current density.

1. Introduction

Carbon nanotubes (CNTs) have long been considered as a promising candidate for electrode materials in lithium ion batteries (LIBs) [1–4]. Comparing with commercialized graphite anode, the tubular, defect-free, and integral structure of pristine CNTs suggests a different mechanism of Li^+ insertion/extraction in contrast to intercalation process to the graphite structure. Experimental work found that pristine single-walled carbon nanotubes (SWCNTs) and multi-walled carbon nanotubes (MWCNTs) showed reversible capacities of only 300 mA h/g [5] and 273 mA h/g [6] after 5 cycles, both were lower than the theoretical capacity of graphite (372 mA h/g in terms of LiC_6). To explain these low capacities, theoretical simulations revealed that the diffusion of Li^+ through the sidewalls of CNTs experienced large energy barriers [7–9]. An ab-initio investigation suggested that such diffusion energy barriers would decrease from 13.5 to 0.5 eV, when topological defects on CNTs were introduced [7]. Therefore, the lithium storage of CNTs is related to a defect-dependent mechanism and the introduction of lateral defects on the CNT sidewalls was identified as an effective strategy to improve the capacity. In this regard, approaches such as chemical etching or mechanical ball milling were explored. For instance, electrochemical measurements of chemically etched and mechanically ball-milled CNTs showed enhanced reversible Li capacities of 681 mA h/g ($Li_{1.8}C_6$) [10] and 641 mA h/g ($Li_{1.7}C_6$) [11]. However, these results were still deficient in terms of long-term cycle stabilities, as only several initial cycles were included. More importantly, further discussions on the long-term performance at a variety of high rate tests were little emphasized.

Another issue in up to date publications involving the electrochemical characterization of CNTs lies in their intrinsic properties. Indeed, the electrochemical performance of CNT is dependent on the morphological factors such as aspect

* *Corresponding authors:* Fax: +86 10 62792457 (Y. Wu), +86 10 62796007 (J. Wang).
E-mail addresses: wuyang.thu@gmail.com (Y. Wu), jpwang@tsinghua.edu.cn (J. Wang).
0008-6223/$ - see front matter
http://dx.doi.org/10.1016/j.carbon.2013.12.047

ratio, curvature, and quality of crystallization. Moreover, the scattered quality of each CNT batch will hardly lead to an unambiguous conclusion. To improve this, we choose super-aligned MWCNTs synthesized in a low-pressure chemical vapor deposition (CVD) system [12–14]. Since the yield and quality of such MWCNTs have met industry-level requirements and the property is quite uniform, stable characterizations of long-term cycle and rate performance could be expected. Another significance is that self-sustained MWCNT films could be directly drawn from super-aligned MWCNT arrays. This mechanical property will guarantee freestanding electrodes in escape of organic binders and conductive additives. Nor metal current collectors are required. Thus, the mass of electrode could be precisely measured and side effects would be minimized. The MWCNT electrodes will be chemically oxidized by two reagents, H_2O_2 and HNO_3, and characterized by transmission electron microscopy (TEM), Raman spectroscopy, and X-ray photoelectron spectroscopy (XPS). In order to better understand the interactions between lithium and MWCNTs, the cycling stabilities of differently treated samples are systematically discussed on the basis of galvanostatic charge and discharge cycles, cyclic voltammetry (CV), and electrochemical impedance spectroscopy (EIS). Finally, the rate performance is also evaluated by applying a series of high current densities to MWCNT electrodes.

2. Experiment

Super-aligned MWCNT arrays on 4-inch silicon wafers with a diameter of 20–30 nm and a height of 300 μm were synthesized in CVD with iron as the catalyst and acetylene as the precursor. The synthesis procedure could be viewed in previous studies [12–14]. The MWCNT film could be drawn from the MWCNT arrays, following an end-to-end joining mechanism, and collected on a stainless steel roller (see in Fig. 1). A razor blade was used to cut off the MWCNT film (inset of Fig. 1).

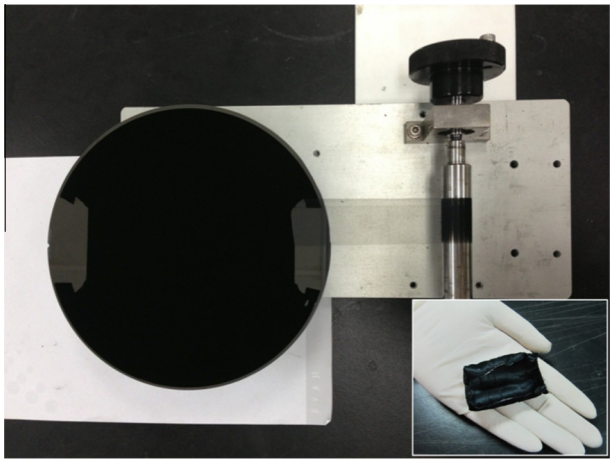

Fig. 1 – Preparation of MWCNT film from MWCNT arrays on a 4-inch silicon wafer with a metallic roller. Inset: photograph of pristine MWCNT sample just cut off from the roller. (A colour version of this figure can be viewed online.)

Chemical modification of MWCNTs was carried out in two different kinds of oxidants, 30 wt.% H_2O_2 and 70 wt.% HNO_3, respectively. For H_2O_2-treated sample, an as-prepared 20 mg MWCNT film was immersed in 50 mL H_2O_2 in a 100 mL round bottom flask. The reaction was then refluxed at 100 °C for 8 h. The resulted MWCNT dispersion was vacuum filtered and washed with distilled water until neutral pH. The sample was finally dried at 80 °C overnight. The HNO_3-treated sample was prepared in a similar condition but only refluxed for 2 h. The sample was also washed with distilled water, and dried at 80 °C overnight. Both treatments would result in freestanding CNT films with yields over 80%.

The morphology and microstructure of chemically modified CNT were studied in a FEI Tecnai G2F20 transmission electron microscope operating at 200 kV. Raman spectra were recorded on a Horiba spectrometer (514 nm Ar laser, 24 mW). XPS analysis was carried out on a Thermal Escalab 250xi spectrometer (50 kV, Al target). C1s XPS spectra were deconvoluted into Gaussian–Lorentzian type peaks after applying a Shirley background.

All electrochemical characterizations were performed in CR2016 coin-type cells that were assembled in an argon-filled glove box (M. Braun Inert Gas Systems Co. Ltd.). Lithium foil was used as the counter electrode for all measurements. A porous polymer film (Celgard 2400, USA) was used as a separator. There was no Cu foil as a current collector in this cell assembly. The electrolyte was 1 M $LiPF_6$ in a mixture of ethylene carbonate and diethyl carbonate with a volumetric ratio of 1:1. The galvanostatic discharge–charge process was measured on a Land battery testing system (Wuhan Land Electronic Co., China) from 0.01 to 3 V. Different specific currents densities ranging from 35 to 3500 mA/g were applied for the different rate characterization. CV experiments were performed on a potentiostat/galvanostat electrochemical system (PARStat 2273) in the voltage range of 0.01 to 3 V with a scan rate of 0.1 mV/s. EIS results were collected on the same apparatus with a perturbation input of 10 mV over the frequency range from 100 kHz to 100 mHz. After electrochemical tests, MWCNT electrodes were taken out and washed with ethanol and distilled water for post-cycle characterizations.

3. Results and discussion

3.1. *Morphological analysis*

The as-grown MWCNT array can be easily drawn into a thin MWCNT film that only consists of single-layered MWCNT yarns arranged in a parallel fashion. The thin MWCNT film was rolled onto a stainless steel cylinder to make freestanding MWCNT electrodes, as shown in Fig. 1. The junction in MWCNTs can be attributed to van der Waals interactions [12]. For oxidized samples, the shape of MWCNT films can be restored after the vacuum filtration process. Fig. 2 showed TEM analysis of the morphology of pristine and chemically modified MWCNTs. The graphitic lattice of pristine MWCNTs can be clearly observed. However, the sidewall was covered with a layer of rough deposit, which was probably a result of hydrocarbon residue during the CVD (see in Fig. 2a). The overall morphology of the chemically modified MWCNTs

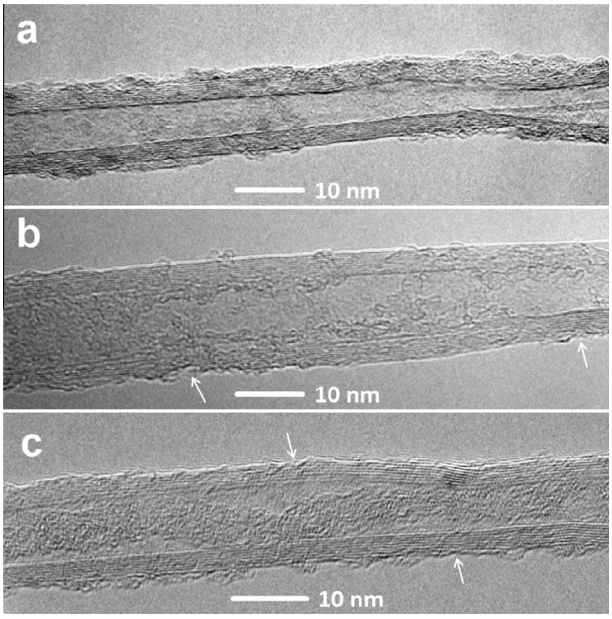

Fig. 2 – TEM images of (a) pristine, (b) H_2O_2-treated, and (c) HNO_3-treated MWCNTs. White arrows indicate surface defects.

was almost the same as that of pristine MWCNT. Further examination revealed that the sidewalls of treated samples were much cleaner than that of pristine MWCNTs, and the layer of hydrocarbon deposit almost disappeared (Fig. 2b and c). Actually, the chemical oxidation has been proved as an effective approach to purify the MWCNT by removing the metal catalyst and the surface deposit [15,16]. Although the surface deposit was almost oxidized, the graphitic lattice was basically maintained, except for some slight imperfections indicated by white arrows in Fig. 2b and c. In addition, the lattice of modified MWCNTs was less pronounced in comparison to pristine ones. Therefore, it strongly suggested that the interactions between oxidants and MWCNTs during the refluxing process would undoubtedly generate surface defects but keep the entire graphitic structure intact.

3.2. *Spectroscopic surface analysis*

Fig. 3 complied Raman spectroscopy analysis for both pristine and modified MWCNTs. Each of the Raman spectra consisted of three characteristic bands, namely the D band at about 1347 cm^{-1}, G band at about 1580 cm^{-1}, and D' band at about 1610 cm^{-1}. The D and D' bands were usually attributed to the presence of amorphous carbon, surface defects, or lattice imperfection and reflected disordering features of MWCNTs. The G band, or the 'graphite' band, originated from in-plane vibrations of carbon atoms with E_{2g} symmetry [17–19]. Therefore, defect concentration in MWCNTs can be estimated in terms of the ratio of intensity of D band and G band (I_D/I_G). As a result, pristine MWCNTs showed an I_D/I_G ratio of 0.605. After oxidization, the intensity D band was obviously pronounced and the I_D/I_G ratios for H_2O_2-treated and HNO_3-treated samples were increased to 0.790 and 1.002, respectively. Thus, we could conclude that the defect concentration of

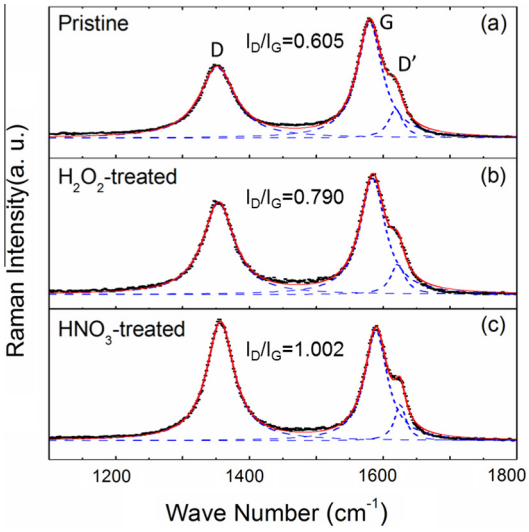

Fig. 3 – Raman spectra of (a) pristine, (b) H_2O_2-treated, and (c) HNO_3-treated MWCNTs. (A colour version of this figure can be viewed online.)

MWCNTs was increased after chemical treatments. This conclusion was also consistent with TEM observations that the chemical oxidation will not only clean the surface of MWCNTs but also create defects in the form of distorted carbon rings or micropores [15].

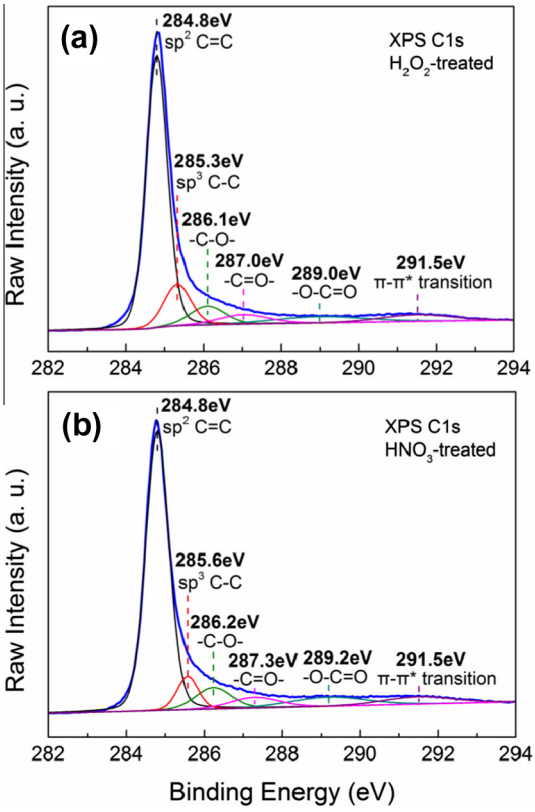

Fig. 4 – Deconvolution of the C1s XPS of (a) H_2O_2-treated and (b) HNO_3-treated MWCNTs. (A colour version of this figure can be viewed online.)

The species of functional groups on the surface of MWCNTs were investigated by XPS. The C1s spectra of H_2O_2-treated and HNO_3-treated samples were shown in Fig. 4. While different chemical reagents were used, both C1s spectra of H_2O_2-treated and HNO_3-treated samples can be deconvoluted into the same number of peaks. The main peak at 284.8 eV was attributed to the graphitic structure composed of sp^2-hybridized C–C bonds. At higher binding energy, a peak at about 285.5 eV appeared as a result of sp^3-hybridized carbon on the defects of the nanotube structure. The surface functionalities can be categorized into three components between 286 and 290 eV, corresponding to hydroxyl, carbonyl, and carboxyl groups (see in Fig. 4). The last component located at 291.5 eV can be attributed to the π–π^* transition [17,20,21]. The same kind of functionalities may suggest the similar mechanism in the oxidizing process, even though different chemical reagents were applied. The intensity of each component was indicative of the concentration of functional groups that attached to the surface of MWCNTs. The amount of oxygen in different treated-MWCNTs could be given as O/C form, the ratio of oxygen contents against carbon contents. According to such analysis, the O/C ratios of H_2O_2-treated and HNO_3-treated MWCNTs were 0.027 and 0.05, respectively. Therefore, the amount of oxygen in the modified MWCNTs would increase when they were oxidized with HNO_3, indicating a high concentration of surface defects. Thus, the XPS analysis was in good agreement the Raman results.

3.3. *Electrochemical characterizations*

3.3.1. *Galvanostatic measurements*

The galvanostatic method was employed to explore the lithium storage capacities of all kinds of MWCNT electrodes. Fig. 5 plotted voltage profiles of the first discharge–charge cycle at a current density of 35 mA/g. All discharge curves dropped rapidly to ca. 0.8 V and leveled off. The voltage plateau at 0.8 V can be attributed to the formation of solid-electrolyte interface (SEI) [22–25]. The coincidence of voltage plateaus for pristine and chemically modified MWCNTs indicated a similar mechanism of SEI growth on the surface of MWCNTs, although both H_2O_2-treated and HNO_3-treated samples contained a number of surface functional groups. The discharge curve was then sloping to the end state of discharging. The irreversible capacity could be estimated as the difference between discharge capacity and charge capacity in the 1st-cycle, while the reversible capacity was taken as the charge capacity in 1st-cycle. The irreversible and reversible capacities of pristine MWCNTs were 665 mA h/g and 241 mA h/g, respectively. For the H_2O_2-treated sample, these values were increased to 852 mA h/g and 334 mA h/g, and further increased to 1186 mA h/g and 488 mA h/g for the HNO_3-treated sample. As shown in Fig. 5, the irreversible process accounted for the most part of discharge capacities of the 1st-cycle. The increase in irreversible capacities indicated more lithium consumption by SEI formation. However, it is worth to note that the increased concentration of surface defects would also enhance the reversible capacities, as manifested in HNO_3-treated samples.

Fig. 6 showed cycle stability up to 80 cycles for all kinds of MWCNTs at the current density of 35 mA/g. All three MWCNT samples exhibited a sharp capacity decrease in the beginning stage but started to deliver stable capacities after 10 cycles. Conversely, the Coulombic efficiency increased from less than 30% for the first cycle to over 90% for the 10th cycle, and then stabilized afterwards (Fig 6b). Such poor Coulombic efficiencies for the first cycle resulted from the irreversible growth of SEI and had been observed in many other nano carbon materials [4,26,27]. After 80 cycles, the cell based on pristine

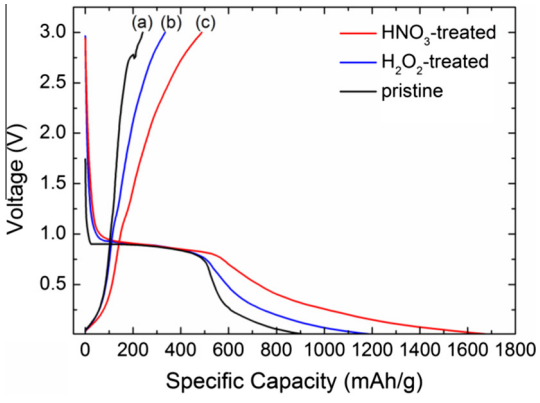

Fig. 5 – The 1st-cycle discharge–charge profiles of pristine and modified MWCNT electrodes. (A colour version of this figure can be viewed online.)

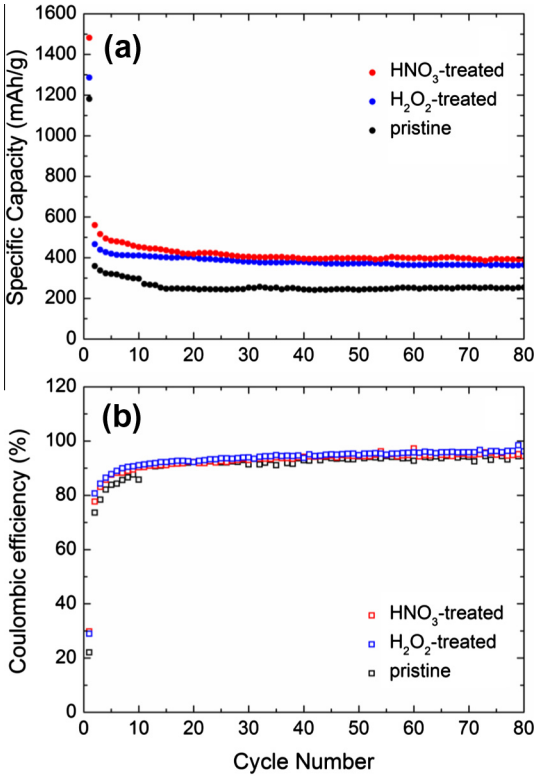

Fig. 6 – (a) Cyclic performance of pristine and modified MWCNTs and (b) Coulombic efficiency at a current density of 35 mA/g and a voltage range of 0.01–3 V. (A colour version of this figure can be viewed online.)

MWCNTs maintained a reversible capacity of 254 mA h/g. Promisingly, H_2O_2-treated and HNO_3-treated samples delivered much better cycle performance than pristine ones throughout the measurement, and exhibited reversible capacities of 364 mA h/g and 391 mA h/g, respectively, at the 80th cycle. It is briefly concluded that MWCNTs would deliver capacities that are competitive with that of commercial graphite (372 mA h/g) after proper chemical modification. Moreover, all kinds of MWCNTs displayed almost the same Coulombic efficiencies and little capacity fading in long-term cycle tests.

3.3.2. *CV, EIS and post-cycle characterizations*

CV measurements were used to explore the lithium insertion/extraction process in H_2O_2-treated and HNO_3-treated samples, as plotted in Fig. 7. Both Fig. 7a and b showed a sharp cathodic peak during the initial discharging process. Compared with voltage profiles in Fig. 5, the onsets of the peak were in good agreement with the voltage of the plateaus. Thus, this peak could be assigned to the formation SEI during the lithiation process. Such cathodic peaks disappeared from the 2nd cycle, indicating that SEI became stable and had little effects on the capacities in proceeding cycles. As a result, both H_2O_2-treated and HNO_3-treated samples displayed similar CV curves for the 2nd cycle. Whereas the peak positions were almost the same, the area differences measured the amount of SEI. By comparing cathodic curves of Fig. 7a and b, it is clear that the more enrichment of defects and functional groups on the surface of HNO_3-treated samples would result in both increased irreversible and reversible capacities.

In order to further explore the electrochemical processes of H_2O_2-treated and HNO_3-treated MWCNTs, impedance spectra were recorded before and after CV tests (Fig. 8). The EIS results of H_2O_2-treated and HNO_3-treated MWCNTs commonly featured depressed semicircles, followed by straight lines with a near 45° slope to the real axis. The spectra could be recognized as the following three processes during lithium insertion into MWCNTs: a charge-transfer process between the CNT electrode and the electrolyte at high frequency region, a migration process of lithium ions on the CNT electrode surface at intermediate frequency region, and a solid-state Li^+ diffusion process into electrode materials at low frequency region [28]. After the CV test, the sizes of semicircles of both H_2O_2-treated and HNO_3-treated MWCNT electrodes significantly decreased. This observation might indicate that chemically treated MWCNTs were more favorable for Li^+ transfer and diffusion at the electrolyte/electrode interface [29].

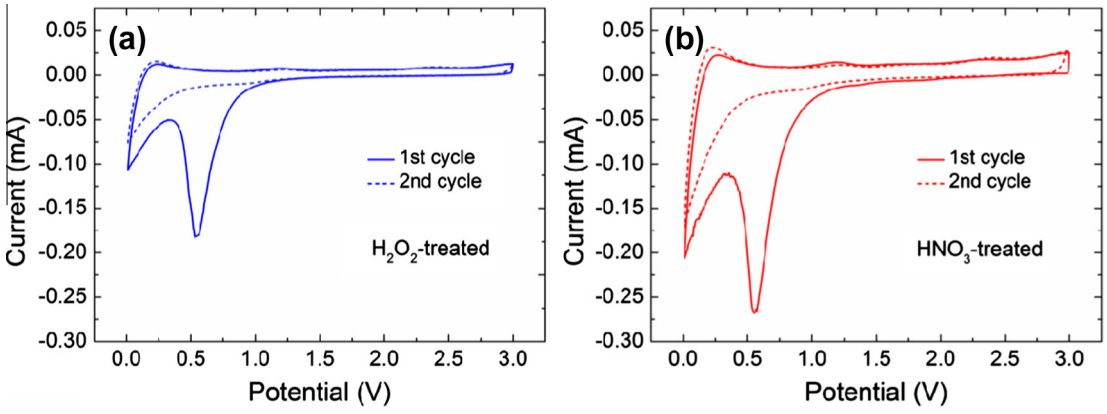

Fig. 7 – CV profiles of (a) H_2O_2-treated and (b) HNO_3-treated CNTs. (A colour version of this figure can be viewed online.)

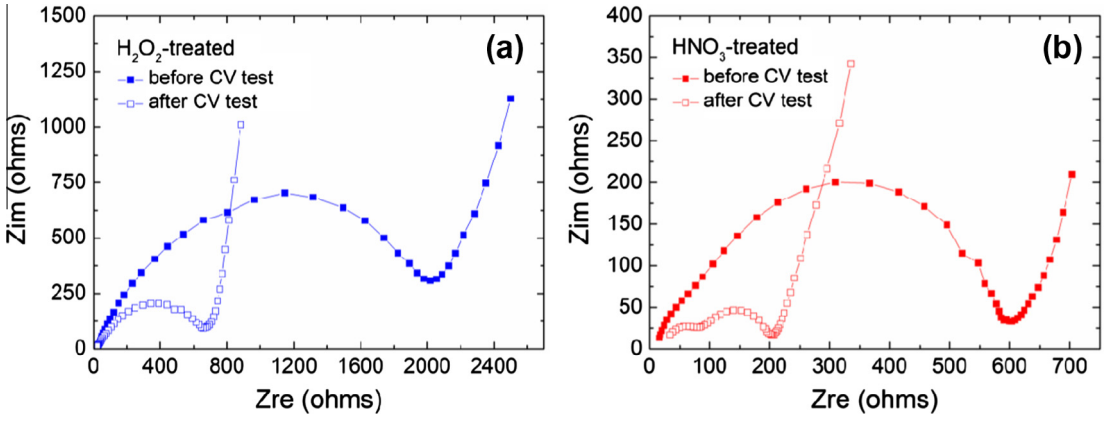

Fig. 8 – Impedance spectra of (a) H_2O_2-treated and (b) HNO_3-treated MWCNTs before and after CV test. (A colour version of this figure can be viewed online.)

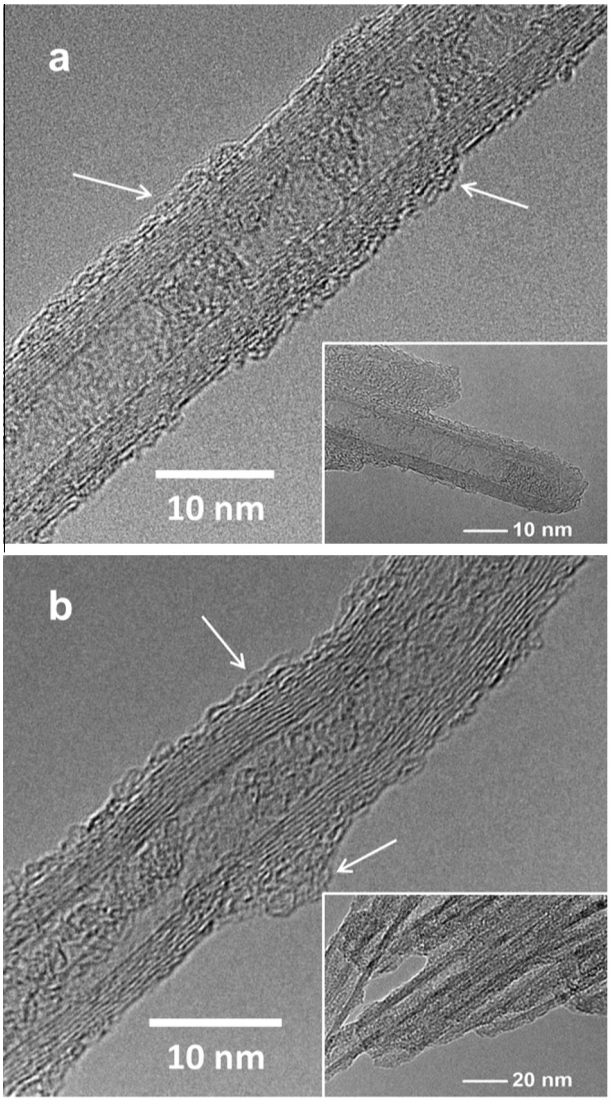

Fig. 9 – TEM images of (a) H_2O_2-treated (b) HNO_3-treated MWCNTs after CV test. Residue of electrolyte was indicated by white arrows. Insets of (a) and (b): MWCNTs with etched or opened ends.

To gain a further understanding to the impact of electrochemical process on MWCNT samples, the post-cycle TEM images of H_2O_2-treated and HNO_3-treated MWCNT electrodes were collected (Fig. 9). The electrochemical process did not modify the surface structure significantly (Please note that the deposit on the surface might arise from unwashed SEI layer, as indicated by white arrows in Fig. 9a and b). However, the end of MWCNTs was much more vulnerable with respect to the electrochemical process. As a result, CNTs with etched or opened ends were observed in TEM for both H_2O_2-treated and HNO_3-treated samples. Remarkably, there were a greater number of open-end tubes in the HNO_3-treated samples in comparison with those H_2O_2-treated samples (insets of Fig. 9a and b). Indeed, post-cycle Raman study provided clear evidences. After such electrochemical cycles, I_D/I_G of H_2O_2-treated samples increased little from 0.792 to 0.832, while that of HNO_3-treated sample greatly increased from 1.002 to 1.206

Table 1 – I_D/I_G intensity ratios of MWCNTs before and after cycling.

Sample	Pristine	H_2O_2-treated	HNO_3-treated
Before cycling	0.605	0.79	1.002
After cycling	0.622	0.832	1.206

(Table 1). Please note that I_D/I_G of pristine MWCNTs just increased from 0.605 to 0.622, indicating that new defects were likely generated on the basis of existing ones. The difference of the change in I_D/I_G strongly indicated that HNO_3-treated samples underwent the highest degree of surface damage, due to the highest initial surface defect concentration. Although the lithium interaction may cause more surface defects, these damages would only be restricted to the outer wall and caps of MWCNTs and no significant number of shortened segments was found in TEM studies. As a matter of fact, both long-term capacity retention and cycle reversibility were pertained. The higher concentration of surface defects and the greater number of opened ends in HNO_3-treated MWCNTs may further decrease the energy barriers and thus resulted in a reduced charge transfer resistance (cf. Fig. 8b). Accordingly, it may suggest distinct kinetics in high current density tests for H_2O_2-treated and HNO_3-treated MWCNTs, with respect to those untreated.

3.3.3. *Rate performance*

Fig. 10 showed the rate performance of pristine and chemically modified MWCNT electrodes at current densities up to

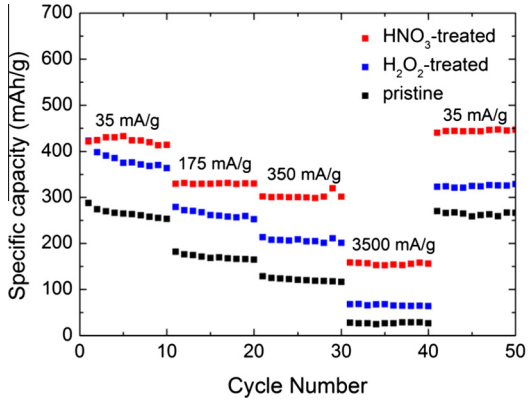

Fig. 10 – Rate performance of pristine and chemically treated MWCNTs. Current density from 35 to 3500 mA/g. Voltage range from 0.01 to 3 V. (A colour version of this figure can be viewed online.)

Table 2 – Reversible capacities (mA h/g) of MWCNTs at different current densities.

	35 mA/g	175 mA/g	350 mA/g	3500 mA/g
Pristine	265	171	121	27
H_2O_2-treated	382	264	206	66
HNO_3-treated	424	330	302	156

3500 mA/g. The reversible capacities of different samples under each current density were compared in Table 2. Pristine MWCNTs presented a specific capacity of 265 mA h/g at a current density of 35 mA/g and but it rapidly decreased to 27 mA h/g when the current density reached 3500 mA/g. H_2O_2-treated samples exhibited a specific capacity of 382 mA h/g at the initial current density and dropped to 264 mA h/g, 206 mA/g, and 66 mA h/g, at current densities of 175 mA/g, 350 mA/g and 3500 mA/g. With respect to HNO_3-treated samples, a much better capacity retention was observed. A high reversible capacity of 424 mA h/g was delivered at 35 mA/g. As the current density increased, it slowly decreased to 330 mA h/g and 302 mA h/g at current densities of 175 mA/g and 350 mA/g. At the highest current density of 3500 mA/g, the HNO_3-treated MWCNT electrode can still deliver a capacity of 156 mA h/g, corresponding to a capacity retention of 37% of its initial values. More importantly, the reversible capacity of HNO_3-treated samples can be reinstalled to 445 mA h/g when the current density returned to 35 mA/g. In contrast, pristine MWCNTs only delivered a poor capacity of 27 mA h/g at such a high current density. The slight increase in the specific capacity (from 424 to 440 mA h/g) for HNO_3-treated MWCNTs after 40 cycles, as shown in Fig. 10, might be attributed to the increase of defects concentration. Raman spectra showed that the I_D/I_G ratio of HNO_3-treated MWCNTs increased to 1.219 after the rate test, higher than those after the cycle test. We assumed that MWCNTs were subject to a greater lattice strains for Li^+ insertion/extraction at higher current densities, but the exact mechanism of surface defects propagation was still unclear. The specific capacity of pristine MWCNTs varied only by 5 mA h/g, and no changes in I_D/I_G were found after the rate test. The H_2O_2-treated MWCNTs exhibited a slight decrease in specific capacity after the high current density tests. The sample inhomogeneity was still an uncontrollable factor, even though we have used rather uniform super-aligned MWCNTs. In comparison with pristine MWCNTs, the higher capacity delivered at all current densities by chemically treated samples could not only be attributed to the increased number of active sites that linked with the concentration of surface defects, but also result from the change in surface polarity that may improve the interaction between ions in the electrolyte and the surface of solid electrodes. The comparison between chemically treated samples revealed that improvement in the rate capability of MWCNTs was a function of the extent of oxidation, which might also lower the energy barrier of Li^+ diffusion in MWCNTs.

4. Conclusion

We systematically characterized and explored electrochemical properties of pristine and chemically treated super-aligned MWCNTs. It was found that the oxidizing treatment would increase the defects concentration and introduce oxygen functionalities on MWCNTs. Electrochemical tests showed that both H_2O_2-treated and HNO_3-treated MWCNTs displayed a sharp distinction in both cycle stability and rate capability compared with pristine MWCNTs. H_2O_2-treated MWCNTs maintained a specific capacity of 364 mA h/g after 80 cycles, while HNO_3-treated MWCNTs maintained an specific capacity of 391 mA h/g. For rate performance, H_2O_2-treated MWCNTs displayed a capacity of 66 mA h/g at a high current density of 3500 mA/g. Remarkably, HNO_3-treated MWCNTs revealed a much higher capacity of 156 mA h/g at this current density, which was almost seven times that of pristine MWCNTs. Thus, appropriate chemical treatments would strengthen the promise of MWCNTs as a potential electrode material for LIBs. Although MWCNTs do not have a potential plateau, their capacitor-like behavior indicates that the capacity could be easily monitored by the potential. Hence, they may find special advantages in the fields where the voltage output is less important than the capacity contained inside the battery, e.g., stationary energy storage facilities. Finally, specific capacities of MWCNTs in the voltage range from 0.01 to 3 V were provided at a variety of charging/discharging rates, and, more importantly, these results could be utilized as valuable references to estimate the practical contribution from MWCNT in composite electrodes, specifically when they were exploited as anode materials.

Acknowledgements

This work was supported by the National Basic Research Program of China (2012CB932301), the NSFC (51102146) and the Chinese Postdoctoral Science Foundation (2012M520261).

REFERENCES

[1] Che G, Lakshmi BB, Fisher ER, Martin CR. Carbon nanotubule membranes for electrochemical energy storage and production. Nature 1998;393(6683):346–9.
[2] Landi BJ, Ganter MJ, Cress CD, DiLeo RA, Raffaelle RP. Carbon nanotubes for lithium ion batteries. Energy Environ Sci 2009;2(6):638–54.
[3] Baughman RH, Zakhidov AA, de Heer WA. Carbon nanotubes–the route toward applications. Science 2002;297(5582):787–92.
[4] Wu YP, Rahm E, Holze R. Carbon anode materials for lithium ion batteries. J Power Sources 2003;114(2):228–36.
[5] Claye AS, Fischer JE, Huffman CB, Rinzler AG, Smalley RE. Solid-state electrochemistry of the Li single wall carbon nanotube system. J Electrochem Soc 2000;147(8):2845–52.
[6] Frackowiak E, Gautier S, Gaucher H, Bonnamy S, Beguin F. Electrochemical storage of lithium in multiwalled carbon nanotubes. Carbon 1999;37(1):61–9.
[7] Meunier V, Kephart J, Roland C, Bernholc J. Ab initio investigations of lithium diffusion in carbon nanotube systems. Phys Rev Lett 2002;88(7):075506.
[8] Zhao J, Buldum A, Han J, Lu JP. First-principles study of Li-intercalated carbon nanotube ropes. Phys Rev Lett 2000;85(8):1706.
[9] Lin K, Xu Y, He G, Wang X. The kinetic and thermodynamic analysis of Li ion in multi-walled carbon nanotubes. Mater Chem Phys 2006;99(2):190–6.
[10] Eom JY, Kwon HS, Liu J, Zhou O. Lithium insertion into purified and etched multi-walled carbon nanotubes synthesized on supported catalysts by thermal CVD. Carbon 2004;42(12):2589–96.
[11] Eom JY, Kim DY, Kwon HS. Effects of ball-milling on lithium insertion into multi-walled carbon nanotubes synthesized by

thermal chemical vapour deposition. J Power Sources 2006;157(1):507–14.
[12] Jiang KL, Li QQ, Fan SS. Nanotechnology: spinning continuous carbon nanotube yarns. Nature 2002;419(6909). 801-801.
[13] Zhang XB, Jiang KL, Feng C, Liu P, Zhang L, Kong J, et al. Spinning and processing continuous yarns from 4-inch wafer scale super-aligned carbon nanotube arrays. Adv Mater 2006;18(12):1505–10.
[14] Jiang K, Wang J, Li Q, Liu L, Liu C, Fan S. Superaligned carbon nanotube arrays, films, and yarns: a road to applications. Adv Mater 2011;23(9):1154–61.
[15] Hou PX, Liu C, Cheng HM. Purification of carbon nanotubes. Carbon 2008;46(15):2003–25.
[16] Choi WK, Park SG, Takahashi H, Cho TH. Purification of carbon nanofibers with hydrogen peroxide. Synth Met 2003;139(1):39–42.
[17] Datsyuk V, Kalyva M, Papagelis K, Parthenios J, Tasis D, Siokou A, et al. Chemical oxidation of multiwalled carbon nanotubes. Carbon 2008;46(6):833–40.
[18] Balasubramanian K, Burghard M. Chemically functionalized carbon nanotubes. Small 2005;1(2):180–92.
[19] Jin SH, Park YB, Yoon KH. Rheological and mechanical properties of surface modified multi-walled carbon nanotube-filled PET composite. Compos Sci Technol 2007;67(15):3434–41.
[20] Okpalugo TIT, Papakonstantinou P, Murphy H, McLaughlin J, Brown NMD. High resolution XPS characterization of chemical functionalised MWCNTs and SWCNTs. Carbon 2005;43(1):153–61.
[21] Gong H, Kim ST, Lee JD, Yim S. Simple quantification of surface carboxylic acids on chemically oxidized multi-walled carbon nanotubes. Appl Surf Sci 2013;266:219–24.
[22] Frackowiak E, Beguin F. Electrochemical storage of energy in carbon nanotubes and nanostructured carbons. Carbon 2002;40(10):1775–87.
[23] Wu GT, Wang CS, Zhang XB, Yang HS, Qi ZF, He PM, et al. Structure and lithium insertion properties of carbon nanotubes. J Electrochem Soc 1999;146(5):1696–701.
[24] Lu W, Chung DDL. Anodic performance of vapor-derived carbon filaments in lithium-ion secondary battery. Carbon 2001;39(4):493–6.
[25] Spahr ME, Palladino T, Wilhelm H, Würsig A, Goers D, Buqa H, et al. Exfoliation of graphite during electrochemical lithium insertion in ethylene carbonate-containing electrolytes. J Electrochem Soc 2004;151(9):A1383–95.
[26] Lee KT, Lytle JC, Ergang NS, Oh SM, Stein A. Synthesis and rate performance of monolithic macroporous carbon electrodes for lithium-ion secondary batteries. Adv Funct Mater 2005;15(4):547–56.
[27] Pan D, Wang S, Zhao B, Wu M, Zhang H, Wang Y, et al. Li storage properties of disordered graphene nanosheets. Chem Mater 2009;21(14):3136–42.
[28] Yang ZH, Wu HQ. The electrochemical impedance measurements of carbon nanotubes. Chem Phys Lett 2001;343(3):235–40.
[29] Yang SB, Song HH, Chen XH, Okotrub AV, Bulusheva LG. Electrochemical performance of arc-produced carbon nanotubes as anode material for lithium-ion batteries. Electrochim Acta 2007;52(16):5286–93.